inorganics

MDPI

Article

Lu-Lu Bond in $Lu_2@C_{60}$ Metallofullerenes

Yaoxiao Zhao [1], Wangqiang Shen [2,3,*], Weixing Chen [1] and Xing Lu [3,*]

[1] Engineering Research Center of Light Stabilizers for Polymer Materials, School of Materials Science and Chemical Engineering, Xi'an Technological University, Xi'an 710021, China; zhaoyaoxiao@xatu.edu.cn (Y.Z.); chenwx@xatu.edu.cn (W.C.)
[2] School of Materials Science and Engineering, Hefei University of Technology, Hefei 230009, China
[3] State Key Laboratory of Materials Processing and Die & Mould Technology, School of Materials Science and Engineering, Huazhong University of Science and Technology, 1037 Luoyu Road, Wuhan 430074, China
* Correspondence: shenwq@hfut.edu.cn (W.S.); lux@hust.edu.cn (X.L.)

Abstract: This study on $Lu_2@C_{60}$ isomers provides insights into the metal–metal bond through the confinement effect of fullerene cages. Density functional theory calculations were used to study the nature of the Lu-Lu bond in two stable endohedral metallofullerenes (EMFs), $Lu_2@C_{2v}$_C_{60} and $Lu_2@I_h$_C_{60}, both with negative endohedral energy. These two isomers are geometrically connected through a simple Stone–Wales (SW) transformation. The electronic configuration of $(Lu_2)^{4+}@C_{60}{}^{4-}$ was also confirmed, leading to the formation of a two-center two-electron (2c–2e) Lu-Lu σ single bond. By comparing the Lu-Lu bonds in $Lu_2@C_{60}$ with those in acknowledged $Lu_2@C_{2n}$, the smaller C_{60} fullerene compressed the geometry of Lu_2 resulting in a much shorter Lu-Lu bond length. However, the Lu-Lu bond strength is slightly weaker in $Lu_2@C_{60}$ than that in large fullerenes, as the Lu-Lu bond in C_{60} is likely a p-p σ bond with an above the 40% contribution of p orbital and a strong metal–cage interaction. Additionally, the vis-NIR spectra of $Lu_2@C_{2v}$_C_{60} and $Lu_2@I_h$_C_{60} were simulated, which could provide valuable information for future experimental studies on Lu-based EMFs.

Keywords: endohedral metallofullerenes; metal–metal bond; size effect

check for updates

Citation: Zhao, Y.; Shen, W.; Chen, W.; Lu, X. Lu-Lu Bond in $Lu_2@C_{60}$ Metallofullerenes. *Inorganics* **2023**, *11*, 277. https://doi.org/10.3390/inorganics11070277

Academic Editor: David Turner

Received: 31 May 2023
Revised: 22 June 2023
Accepted: 26 June 2023
Published: 28 June 2023

1. Introduction

Metal–metal bonds have been a subject of significant research interest in past decades, which show important roles in catalysis and biology [1,2]. Metal–metal bonds provide a large perturbation in electronic structure and the unique properties of these dinuclear fragments can be harnessed in a broad range of applications [3]. Since the synthesis and characterization of $Re_2Cl_8{}^{2-}$ [4], there is growing evidence for the formation of metal–metal bonds under specific conditions [5,6], and growing research interest in understanding the nature of the metal–metal bonds. Generally, the transition metals could form multinuclear complexes with direct metal–metal interactions, but a complex coordination environment makes it difficult to understand the nature of metal–metal interaction [7].

Luckily, endohedral dimetallofullerenes (di-EMFs), i.e., fullerenes with two metal atoms trapped inside are considered as the ideal model to study the metal–metal bond [8]. In 2014, di-EMF $Sc_2@C_1(4059)$-C_{66} was determined as the geometry of Sc_2C_{66} molecule by the single-crystal X-ray diffraction (XRD) [9]. $La_2@C_{94}$ are also proposed with experimental and theoretical methods [10], and later, theoretical study revealed that the La–La bond plays a key role in the stability of dimetallofullerenes $[La_2@C_{2n}]^-$ ($2n$ = 92–96) [11]. Recently, Chen et al. have studied Sc-Y σ^2 bond in $ScY@C_{3v}(8)$-C_{82} [12].

Additionally, the previous reports clarified strong confinement effects of fullerene size on the metal-metal bond in EMFs [7,13–15]. For example, Poblet et al. theoretically reveal a U-U triple bond in $U_2@C_{60}$ with the effective bond order of 2.52, singly occupied molecular orbitals (MOs) with metal–metal bond characters in $U_2@C_{80}$, non-negligible U···U interaction in $U_2@C_{78}$, but the metal–metal interaction almost disappears in $U_2@C_{104}$ [8]. In 2017, di-EMFs $Lu_2@C_{2n}$ ($2n$ = 82, 84, and 86) were synthesized and characterized with

the single-crystal XRD method, which gives the crystallographic evidence of direct Lu-Lu bond between two divalent lutetium ions inside fullerenes [16]. Later, additional Lu_2C_{2n} ($2n$ = 76–90) molecules were reported with a wide range cage size, and the successful isolation and unambiguous crystallographic assignment of a series of lutetium-containing EMFs, Lu_2C_{2n} ($2n$ = 76, 78, 80, 84, 86, 88, and 90), reveal an unrecognized decisive effect of the cage size on the configuration of the encapsulated clusters [17]. Following theoretical studies reveal a stable two-center two-electron (2c–2e) Lu-Lu σ bond in $Lu_2@C_{84}$ and $Lu_2@C_{86}$ [18,19]. However, experimental and theoretical study focused on the Lu-containing di-EMFs with medium- or large-size fullerene cages and Lu-Lu bond in small fullerene cages is still unclear.

Herein, Lu-Lu bond is studied in the smaller C_{60} fullerene cage with the highest yield in the fullerene family by using density functional theory calculations and bonding analysis. The aim is to evaluate the confinement effect of fullerene size on the Lu-Lu bond. Two isomers, C_{2v}_C_{60} and I_h_C_{60}, which have been previously verified as the stable host cage of C_{60} fullerene to encage inner moieties, were selected as they have well-established thermodynamic stability and were used to encapsulate the Lu_2 dimer. The bonding features of the Lu-Lu in the C_{60} were evaluated via frontier molecular orbital (FMO), natural bond orbital (NBO), and bond orders analyses. Additionally, the visible-near-infrared (vis-NIR) spectra of $Lu_2@C_{2v}$_C_{60} and $Lu_2@I_h$_C_{60} were simulated to study their electronic features and gain a better understanding of the Lu-Lu bonds both in theory and experiment.

2. Results and Discussion

2.1. Stability and Geometries of $Lu_2@C_{60}$

The good stability of fullerenes C_{2v}_C_{60} and I_h_C_{60}, connected through a single-step Stone-Wales transformation, has been previously reported [20], and they have been characterized as suitable isomers of C_{60} fullerenes to encage metal atoms or clusters [8,21]. In this work, we focus on both $Lu_2@C_{2v}$_C_{60} and $Lu_2@I_h$_C_{60} to generally elucidate the confinement effect of the fullerene on metal–metal bond.

Figure 1 shows the optimized geometries of $Lu_2@C_{2v}$_C_{60} and $Lu_2@I_h$_C_{60}. The lowest frequencies for $Lu_2@C_{2v}$_C_{60} and $Lu_2@I_h$_C_{60} are calculated to be 36 and 45 cm^{-1}, respectively, suggesting their possible existence, as shown in Figures S1 and S2. The single-point energy calculations showed that the $Lu_2@C_{2v}$_C_{60} possessed energy of 5.3 kcal·mol^{-1} higher than the energy of $Lu_2@I_h$_C_{60}, of which results are confirmed by the hybrid functional PBE0 (PBE0/6-311G(d,p)~SDD//PBE0/6-31G(d)~CEP-4G) showing $Lu_2@C_{2v}$_C_{60} with energy of 0.7 kcal·mol^{-1} higher than the energy of $Lu_2@I_h$_C_{60}.

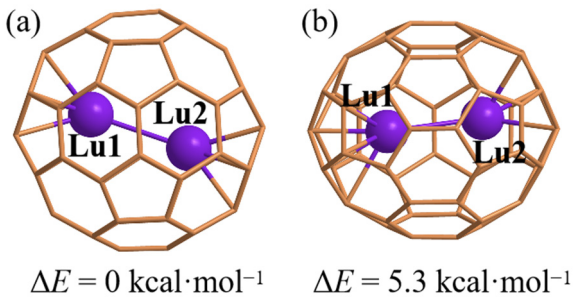

Figure 1. Geometries of optimized $Lu_2@I_h$_C_{60} (**a**) and $Lu_2@C_{2v}$_C_{60} (**b**) on the PBE/6-31G(d)~CEP-4G, including the relative energy (ΔE) on the theoretical level of PBE/6-311G(d,p)~SDD with single-point calculations.

In order to evaluate the effect of temperature, the Boltzmann distribution has been calculated for $Lu_2@C_{2v}$_C_{60} and $Lu_2@I_h$_C_{60}. The results indicate that the Boltzmann distribution of $Lu_2@I_h$_C_{60} is about 97%, 84%, 75%, 70%, 66%, and 63% at 500, 1000, 1500, 2000, 2500, and 3000 K, respectively, which is higher than $Lu_2@C_{2v}$_C_{60} with the Boltzmann distribution values of about 4%, 16%, 25%, 30%, 34%, and 37% at 500, 1000, 1500, 2000,

2500, and 3000 K, respectively. The energy gaps between the highest occupied molecular orbital (HOMO) and the lowest unoccupied molecular orbital (LUMO) are 0.19 and 0.35 eV for $Lu_2@I_h\_C_{60}$ and $Lu_2@C_{2v}\_C_{60}$, respectively, which are larger than the DFT-computed HOMO-LUMO gaps of $Lu_2@C_s(17,490)\_C_{76}$ and $Lu_2@C_{2v}(19,138)\_C_{76}$ [22].

The formation energy for $Lu_2@C_{2v}\_C_{60}$ and $Lu_2@I_h\_C_{60}$ has been calculated by basis set superposition error (BSSE) correction with a counterpoise calculation on the PBE/6-311G(d,p)~SDD considering the Grimme's dispersion with the original D3 damping function. The formation energy for $Lu_2@C_{2v}\_C_{60}$ and $Lu_2@I_h\_C_{60}$ are −179.7 and −156.4 kcal·mol^{-1}, indicating the possible synthesis and isolation in experiment. On the other hand, the much negative formation energy indicates their good stability. The similar stability for $Lu_2@I_h\_C_{60}$ and $Lu_2@C_{2v}\_C_{60}$ might be explained by the geometrical connection with only the single-step Stone–Wales transformation, and this case is similar to the hollow cage of $C_{2v}\_C_{60}$ and $I_h\_C_{60}$ isomers.

The Lu-Lu bond length in $Lu_2@I_h\_C_{60}$ and $Lu_2@C_{2v}\_C_{60}$ are 3.04 and 3.14 Å, respectively, which are much smaller than the previously reported Lu-Lu bond length (~3.50 Å) in $Lu_2@C_{2n}$ ($2n \geq 76$) [17–19,22]. This suggests that there is a confinement effect of fullerenes on the Lu-Lu bond length. The bond length of Sc-Sc and Y-Y in C_{82} are 3.201 and 3.695 Å, respectively, and bond length of La-La in C_{80} is 3.826 Å, indicating the presence of a metal–metal single bond, which has been verified in both theory and experiment [22]. Based on the geometry, further study into the confinement effect of fullerenes on the Lu-Lu bond is warranted.

2.2. Electronic Structures of $Lu_2@C_{60}$

The electronic structure of $Lu_2@C_{60}$ was further investigated through NBO calculations. The results in Table 1 show that there is charge transfer from inner Lu_2 dimer to the C_{60} fullerenes, and in combination with the Lu-Lu σ bond in C_{60}, the 6s orbitals of Lu atoms lose four electrons in $Lu_2@C_{60}$. Therefore, the electronic configurations of both $Lu_2@I_h\_C_{60}$ and $Lu_2@C_{2v}\_C_{60}$ can be expressed as $(Lu_2)^{4+}@(C_{60})^{4-}$.

Table 1. Natural population analysis (NPA) on $Lu_2@I_h\_C_{60}$ and $Lu_2@C_{2v}\_C_{60}$, and the NPA charges (*e*) for metal atoms on the PBE/6-311G(d,p)~SDD.

Molecules	Atoms	Populations	NPA Charges
$Lu_2@I_h\_C_{60}$	Lu1	$5d^{0.37}6s^{0.29}6p^{0.48}6d^{0.88}7p^{0.29}$	0.78
	Lu2	$5d^{0.36}6s^{0.37}6p^{0.46}6d^{0.85}7p^{0.28}$	0.78
$Lu_2@C_{2v}\_C_{60}$	Lu1	$5d^{0.36}6s^{0.30}6p^{0.41}6d^{0.97}7p^{0.39}$	0.65
	Lu2	$5d^{0.34}6s^{0.30}6p^{0.32}6d^{0.89}7p^{0.40}$	0.83

In addition, the location of fractional charge on 6p, 6d, and 7p orbitals of Lu atoms implies the occurrence of back-donation, similar to that observed in other EMFs [23–37]. This is further supported by the presence of electrostatic interaction between the Lu_2 dimer and fullerene cages, as depicted in Figure 2. These observations are consistent with the ionic model of EMFs [13,38,39].

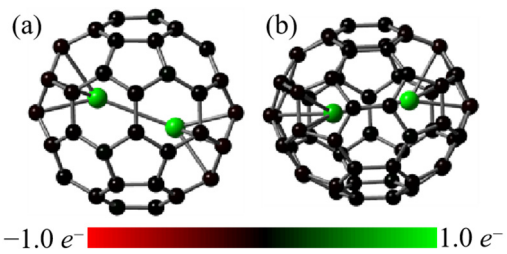

Figure 2. NPA charges for $Lu_2@I_h\_C_{60}$ (**a**) and $Lu_2@C_{2v}\_C_{60}$ (**b**) on the PBE/6-311G(d,p)~SDD, in which the atoms are colored by corresponding NPA charges.

Furthermore, the FMOs have been mapped as shown in Figure 3, in which the C_{60} fullerenes based on single-point calculations are obtained from the optimized $Lu_2@I_h\_C_{60}$ and $Lu_2@C_{2v}\_C_{60}$. The highest occupied molecular orbitals (HOMOs) of $Lu_2@C_{60}$ are contributed by the Lu_2 dimer, presenting the Lu-Lu bond. It is clear that the LUMO and LUMO + 1 of the C_{60} fullerenes become the HOMO-1 and HOMO-2 of the $Lu_2@C_{60}$ indicating the four-electron transfer from inner moiety to fullerene cage, and this result is in line with the natural bond order analysis again confirming the electronic configuration of $(Lu_2)^{4+}@(C_{60})^{4-}$. This electronic configuration has been verified in the previous report on $Lu_2@C_{2n}$ ($2n \geq 76$) [17–19,22]. Additionally, the t_{1u} LUMO has been split after encapsulation of Lu_2 dimer. As shown in Figure 3, after encapsulation of Lu_2 dimer in I_h-C_{60}, its energy level of LUMO + 1 and LUMO is equal, but the energy level of LUMO + 2 is −4.22 eV. This is derived from the distortion of C_{60} fullerene. The symmetry of I_h-C_{60} and C_{2v}-C_{60} have reduced to D_{3d} and C_1, respectively, after encapsulation, and the calculated distortion energies of I_h-C_{60} and C_{2v}-C_{60} are 35.4 and 29.6 kcal·mol^{-1}, respectively, on the theoretical level of PBE/6-311G(d,p)~SDD.

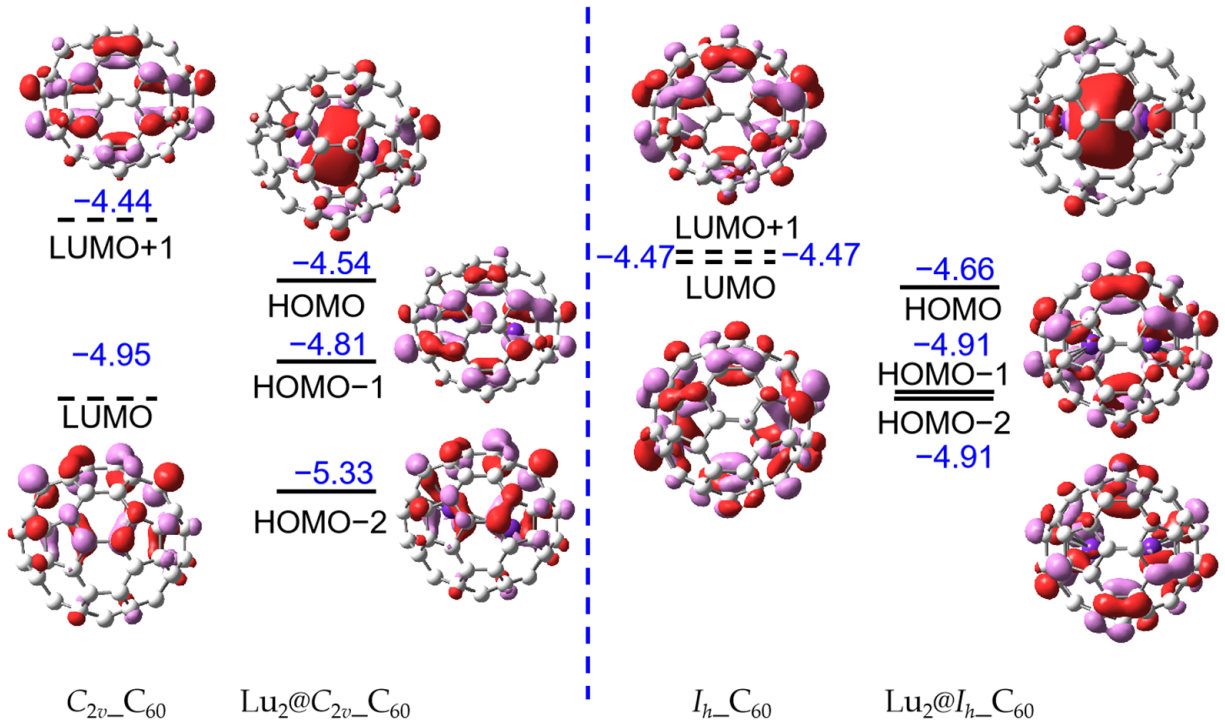

Figure 3. FMOs for stable $C_{2v}\_C_{60}$, $I_h\_C_{60}$, $Lu_2@I_h\_C_{60}$, and $Lu_2@C_{2v}\_C_{60}$ molecules with isovalue of 0.03 a.u. for the surface with the PBE functional, 6-311G(d,p) basis set for carbon atoms, and SDD basis set for Lu atoms. The highest occupied molecular orbitals (HOMO) represented the Lu-Lu bond in C_{60}. The blue numbers represent the energies of orbitals.

2.3. Bonding Features of $Lu_2@C_{60}$

Figure 3 illustrates the presence of a clearly localized bonding molecular orbital between two Lu atoms in $Lu_2@C_{60}$, which has been reported in previous studies [16–19]. The energy level of the bonding molecular orbitals is −4.66 and −4.54 eV for $Lu_2@I_h\_C_{60}$ and $Lu_2@C_{2v}\_C_{60}$, respectively. However, due to the confinement effect of the smaller fullerene cage size, such as C_{60}, further investigation is needed to determine the strength of the Lu-Lu bond. The LUMOs are shown in Figure S3, which display both a metal–metal antibonding orbital and a π antibonding orbital.

To study the nature of the Lu-Lu bond in small fullerene sizes, we calculated the Mayer bond order (MBO) and Wiberg bond order (WBO) and the results are presented in Table 2. Despite the much shorter bond length of Lu-Lu in fullerene C_{60}, the MBO for Lu-Lu bond

in C_{60} is smaller than that in larger fullerenes. For example, in $Lu_2@C_{2n}$ ($2n$ = 84 and 86), the MBO is a little larger than 1 for Lu-Lu bond with a larger bond length [18,19]. The WBOs for Lu-Lu bond in C_{60} are also smaller than 1. To gain further insights into this abnormal phenomenon, the hybrid compositions of M-M bond in $Lu_2@C_{60}$ were studied with NBO calculations. As shown in Table 2, the p orbital contributes more than 40% to the Lu-Lu bond, while the rest of the contributions come from the s and d atomic orbitals. Thus, the Lu-Lu σ bond in C_{60} is likely a p-p σ bond. Previous studies have shown that the Lu-Lu bond is mainly contributed by s orbitals [18,19], in which the metal–metal bond is more like a s-s σ bond. Generally, the overlap of s orbitals is more effective than that of p orbitals, meaning that the s-s σ bond is much stronger than the p-p σ bond. On the other hand, the interaction between Lu_2 dimer and fullerene cage C_{60} is stronger with MBO values of 4.19 and 4.82 for $Lu_2@I_h\_C_{60}$ and $Lu_2@C_{2v}\_C_{60}$, respectively.

Table 2. Mayer bond order (MBO) and Wiberg bond order (WBO) of Lu-Lu bond, and hybrid compositions of M-M bond in the $Lu_2@C_{60}$ at the theoretical level of PBE/6-311G(d,p)~SDD.

Molecules	MBO	WBO	Atoms	Hybrid Composition
$Lu_2@I_h\_C_{60}$	0.99	0.73	Lu1 Lu2	s(26%)p(46%)d(28%) s(36%)p(43%)d(21%)
$Lu_2@C_{2v}\_C_{60}$	0.84	0.67	Lu1 Lu2	s(26%)p(44%)d(30%) s(28%)p(45%)d(27%)

In $Lu_2@I_h\_C_{60}$ and $Lu_2@C_{2v}\_C_{60}$, the Lu-Lu σ bond is mainly derived from p orbitals, for which the bond strength is related to the bond length. The Lu-Lu bond in $I_h\_C_{60}$ with higher values of bond orders (0.99 for MBO and 0.73 for WBO, Table 2) show stronger bond strength than that in $C_{2v}\_C_{60}$, because the shorter bond length in $I_h\_C_{60}$ than that in $C_{2v}\_C_{60}$.

2.4. Simulated Spectra of $Lu_2@C_{60}$

Figure 4 illustrates that the excitation energies of the first excited state of $Lu_2@I_h\_C_{60}$ and $Lu_2@C_{2v}\_C_{60}$ are 0.49 eV (2542 nm) and 0.47 eV (2637 nm), respectively, which are smaller than the first excitation energy of approximately 0.90 eV (1384 nm) for $Lu_2@C_{86}$ in both theory and experiment [16,19]. The excitation form S_0 to S_1 is primarily derived from the transition of electrons from the highest occupied molecular orbital (HOMO) to the lowest unoccupied molecular orbital (LUMO) of $Lu_2@C_{60}$, and the energy required for this transition is 0.78 e^- and 0.61 e^- for $Lu_2@I_h\_C_{60}$ and $Lu_2@C_{2v}\_C_{60}$, respectively. As demonstrated in Figure 3 and Figure S3, the HOMO corresponds to the metal–metal bonding orbital and the LUMO corresponds to the metal–metal antibonding orbital and the π antibonding orbital in $Lu_2@C_{60}$, which is potential reason why their first excitation energy is low. The much lower first excitation energy and the ease of electron transition suggest the poor photochemical stability of $Lu_2@C_{60}$.

In addition, although the absorption peaks of $Lu_2@I_h\_C_{60}$ and $Lu_2@C_{2v}\_C_{60}$ isomers have similar shapes (Figure 4), there is a clear difference in their absorption strength, which can be useful for distinguishing them in the future experiments. Specifically, $Lu_2@I_h\_C_{60}$ exhibits a much stronger absorption peak at around 750 nm compared to $Lu_2@C_{2v}\_C_{60}$. The absorption band at 200–700 nm for $Lu_2@C_{2v}\_C_{60}$ is slightly wider than that of $Lu_2@I_h\_C_{60}$. Furthermore, the IR spectra of $Lu_2@I_h\_C_{60}$ and $Lu_2@C_{2v}\_C_{60}$ were simulated (Figure S4) to evaluate their vibration models. These characterized absorption peaks in the vis-NIR and IR spectra can be beneficial for future characterization of $Lu_2@C_{60}$ in experiments.

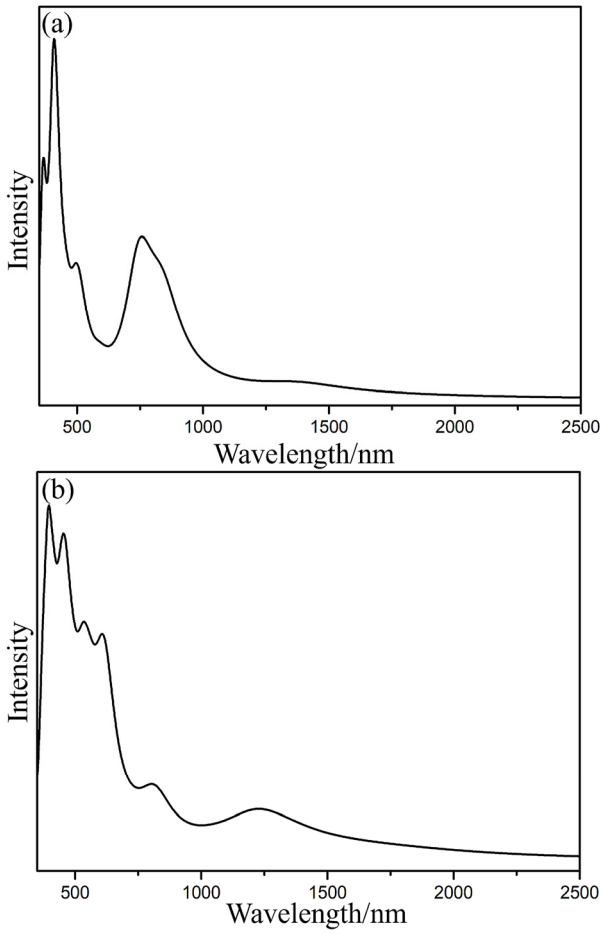

Figure 4. Simulated vis-NIR spectra of the $Lu_2@I_h\_C_{60}$ (**a**) and $Lu_2@C_{2v}\_C_{60}$ (**b**) isomers. The broadening function is Lorentzian and full width at half maximum is 0.30 eV.

3. Computational Methods

The optimizations of $Lu_2@C_{2v}\_C_{60}$ and $Lu_2@I_h\_C_{60}$ were carried out on the PBE/6-31G(d)~CEP-4G theoretical level [40,41], in which the basis function 6-31G(d) was used for the carbon atom and CEP-4G containing pseudopotential was used for the lutetium atom with valance electronic configuration of $4f^{14}5d^16s^2$. The frequencies were calculated on the same theoretical level for the optimized geometries of $Lu_2@C_{60}$, and all of them are free from imaginary frequency meaning the existence of local minima point for $Lu_2@C_{2v}\_C_{60}$ and $Lu_2@I_h\_C_{60}$. The PBE has been previously proved to be the suitable functional for the lutetium-based EMFs [18,19,42,43]. To obtain accurate energy and frontier molecular orbitals (FMOs), a single-point calculation was performed on the PBE/6-311G(d,p)~SDD theoretical level, in which a larger basis set 6-311G(d,p) [40] with polarization functions and SDD with effective core pseudopotential were used for the carbon and lutetium atoms, respectively. In order to confirm the calculated results on PBE, the hybrid functional PBE0 (PBE0/6-311G(d,p)~SDD//PBE0/6-31G(d)~CEP-4G) calculations were also carried out for both $Lu_2@C_{2v}\_C_{60}$ and $Lu_2@I_h\_C_{60}$. In order to evaluate the effect of temperature, the Boltzmann distribution has been calculated for $Lu_2@C_{2v}\_C_{60}$ and $Lu_2@I_h\_C_{60}$. The formation energy for $Lu_2@C_{2v}\_C_{60}$ and $Lu_2@I_h\_C_{60}$ was calculated based on basis set superposition errors via counterpoise corrections on the theoretical level of PBE/6-311G(d,p)~SDD. NBO [44] analyses were also conducted on the PBE/6-311G(d,p)~SDD theoretical level. The vis-NIR spectra were simulated on the PBE/6-31G(d)~CEP-4G theoretical level. All the above calculations were carried out by Gaussian16 software package [45]. In addition, Mayer bond order (MBO) [46] together with localized molecular orbitals (LMOs) [47,48] analyses for $Lu_2@C_{60}$ were performed with the Multiwfn program [49].

4. Conclusions

Based on the $Lu_2@I_h\_C_{60}$ and $Lu_2@C_{2v}\_C_{60}$ which are related by a single-step Stone–Wales transformation, we provide insight into the confinement effects of fullerene on the metal–metal bonding. Although, in the $Lu_2@C_{60}$, there is a much shorter Lu-Lu bond length, its bond strength is a little weaker than the Lu-Lu bond in large fullerenes, because the Lu-Lu σ bond in C_{60} is likely a p-p σ bond with the contribution p orbital above 40% and a strong metal–cage interaction. Clearly, the confinement effects of fullerene play important roles in the geometry of the inner cluster, especially the bond length in the present work, and the electronic effect is more important for the bonding nature. Furthermore, the electronic configurations of $(Lu_2)^{4+}@C_{60}{}^{4-}$ were confirmed. Additionally, the vis-NIR spectra of $Lu_2@C_{2v}\_C_{60}$ and $Lu_2@I_h\_C_{60}$ were simulated, which could give some valuable information for the future experimental study on Lu-based EMFs.

Supplementary Materials: The following supporting information can be downloaded at: https://www.mdpi.com/article/10.3390/inorganics11070277/s1, Figure S1: Several selected displacement vectors of $Lu_2@I_h\_C_{60}$ with vibration frequencies, including the lowest vibration one; Figure S2: Several selected displacement vectors of $Lu_2@C_{2v}\_C_{60}$ with vibration frequencies, including the lowest vibration one; Figure S3: Lowest unoccupied molecular orbitals (LUMO) with localization of $Lu_2@I_h\_C_{60}$ (a) and $Lu_2@C_{2v}\_C_{60}$ (b) with isovalue of 0.03 a.u. for the surface; Figure S4: IR vibration spectra for $Lu_2@I_h\_C_{60}$ (a) and $Lu_2@C_{2v}\_C_{60}$ (b). The broadening function is Gaussian function and full width at half maximum is 12 cm^{-1}; coordinates for optimized geometries: $Lu_2@I_h\_C_{60}$ and $Lu_2@C_{2v}\_C_{60}$.

Author Contributions: Conceptualization, X.L. and W.S.; methodology, Y.Z.; software, Y.Z.; validation, X.L., W.S., W.C. and Y.Z.; formal analysis, Y.Z. and W.S.; investigation, Y.Z.; data curation, Y.Z.; writing—original draft preparation, Y.Z. and W.S.; writing—review and editing, W.C. and X.L.; visualization, Y.Z.; supervision, X.L.; project administration, X.L.; funding acquisition, X.L. and W.S. All authors have read and agreed to the published version of the manuscript.

Funding: This research was funded by the National Natural Science Foundation of China (21925104, 22001084, and 92261204).

Data Availability Statement: Data are available on request from the authors.

Acknowledgments: We thank the Analytical and Testing Center at the Hefei University of Technology and Huazhong University of Science and Technology for all related measurements, and national supercomputing center in Xi'an.

Conflicts of Interest: The authors declare no conflict of interest.

References

1. Rodriguez, J.A.; Goodman, D.W. The nature of the metal-metal bond in bimetallic surfaces. *Science* **1992**, *257*, 897–903. [CrossRef] [PubMed]
2. Lindahl, P.A. Metal–metal bonds in biology. *J. Inorg. Biochem.* **2012**, *106*, 172–178. [CrossRef] [PubMed]
3. Powers, I.G.; Uyeda, C. Metal–metal bonds in catalysis. *ACS Catal.* **2017**, *7*, 936–958. [CrossRef]
4. Cotton, F.A. Strong homonuclear metal-metal bonds. *Acc. Chem. Res.* **1969**, *2*, 240–247. [CrossRef]
5. Foroutan-Nejad, C.; Vicha, J.; Marek, R.; Patzschke, M.; Straka, M. Unwilling U-U bonding in $U_2@C_{80}$: Cage-driven metal-metal bonds in di-uranium fullerenes. *Phys. Chem. Chem. Phys.* **2015**, *17*, 24182–24192. [CrossRef] [PubMed]
6. Zhuang, J.; Morales-Martínez, R.; Zhang, J.; Wang, Y.; Yao, Y.R.; Pei, C.; Rodríguez-Fortea, A.; Wang, S.; Echegoyen, L.; de Graaf, C.; et al. Characterization of a strong covalent Th^{3+}-Th^{3+} bond inside an $I_h(7)$-C_{80} fullerene cage. *Nat. Commun.* **2021**, *12*, 2372. [CrossRef]
7. Li, M.; Zhao, R.; Dang, J.; Zhao, X. Theoretical study on the stabilities, electronic structures, and reaction and formation mechanisms of fullerenes and endohedral metallofullerenes. *Coordin. Chem. Rev.* **2022**, *471*, 214762. [CrossRef]
8. Moreno-Vicente, A.; Roselló, Y.; Chen, N.; Echegoyen, L.; Dunk, P.W.; Rodríguez-Fortea, A.; de Graaf, C.; Poblet, J.M. Are U–U Bonds Inside Fullerenes Really Unwilling Bonds? *J. Am. Chem. Soc.* **2023**, *145*, 6710–6718. [CrossRef]
9. Yamada, M.; Kurihara, H.; Suzuki, M.; Guo, J.D.; Waelchli, M.; Olmstead, M.M.; Balch, A.L.; Nagase, S.; Maeda, Y.; Hasegawa, T. $Sc_2@C_{66}$ revisited: An endohedral fullerene with scandium ions nestled within two unsaturated linear triquinanes. *J. Am. Chem. Soc.* **2014**, *136*, 7611–7614. [CrossRef]
10. Zhao, S.; Zhao, P.; Cai, W.; Bao, L.; Chen, M.; Xie, Y.; Zhao, X.; Lu, X. Stabilization of Giant Fullerenes $C_2(41)$-C_{90}, $D_3(85)$-C_{92}, $C_1(132)$-C_{94}, $C_2(157)$-C_{96}, and $C_1(175)$-C_{98} by Encapsulation of a Large La_2C_2 Cluster: The Importance of Cluster–Cage Matching. *J. Am. Chem. Soc.* **2017**, *139*, 4724–4728. [CrossRef]

11. Li, Q.-Z.; Zheng, J.-J.; He, L.; Nagase, S.; Zhao, X. La–La bonded dimetallofullerenes $[La_2@C_{2n}]^-$: Species for stabilizing C_{2n} ($2n$ = 92–96) besides $La_2C_2@C_{2n}$. *Phys. Chem. Chem. Phys.* **2018**, *20*, 14671–14678. [CrossRef] [PubMed]
12. Zheng, L.; Roselló, Y.; Yan, Y.; Yao, Y.R.; Fan, X.; Poblet, J.M.; Rodríguez-Fortea, A.; Chen, N. ScY@C_{3v}(8)-C_{82}: Metal-Metal σ^2 Bond in Mixed Rare-Earth Di-metallofullerenes. *Chin. J. Chem.* 2023; *early view*. [CrossRef]
13. Popov, A.A.; Yang, S.; Dunsch, L. Endohedral fullerenes. *Chem. Rev.* **2013**, *113*, 5989–6113. [CrossRef]
14. Lu, X.; Akasaka, T.; Nagase, S. Chemistry of endohedral metallofullerenes: The role of metals. *Chem. Commun.* **2011**, *47*, 5942–5957. [CrossRef]
15. Shen, W.; Bao, L.; Lu, X. Endohedral Metallofullerenes: An Ideal Platform of Sub-Nano Chemistry. *Chin. J. Chem.* **2022**, *40*, 275–284. [CrossRef]
16. Shen, W.; Bao, L.; Wu, Y.; Pan, C.; Zhao, S.; Fang, H.; Xie, Y.; Jin, P.; Peng, P.; Li, F.-F. $Lu_2@C_{2n}$ ($2n$ = 82, 84, 86): Crystallographic evidence of direct Lu–Lu bonding between two divalent lutetium ions inside fullerene cages. *J. Am. Chem. Soc.* **2017**, *139*, 9979–9984. [CrossRef] [PubMed]
17. Shen, W.; Bao, L.; Hu, S.; Yang, L.; Jin, P.; Xie, Y.; Akasaka, T.; Lu, X. Crystallographic characterization of Lu_2C_{2n} ($2n$ = 76–90): Cluster selection by cage size. *Chem. Sci.* **2019**, *10*, 829–836. [CrossRef]
18. Zheng, H.; Dang, H.; Zhao, Y.; Gu, Y.-X.; Li, M.; Li, Q.-Z.; Zhao, X. Theoretical Investigations of Lu_2C_{84}: Unexpected Impact of Metal Electronic Configuration toward the Metal–Metal σ-Bond in Fullerene. *Inorg. Chem.* **2020**, *59*, 10113–10122. [CrossRef]
19. Zhang, K.; Zheng, H.; Li, M.; Li, Q.-Z.; Zhao, Y.; Zhao, X. Significant roles of a particularly stable two-center two-electron Lu–Lu σ bond in $Lu_2@C_{86}$: Electronic structure of Lu and radius of Lu^{2+}. *Inorg. Chem.* **2021**, *60*, 2425–2436. [CrossRef]
20. Stone, A.J.; Wales, D.J. Theoretical studies of icosahedral C_{60} and some related species. *Chem. Phys. Lett.* **1986**, *128*, 501–503. [CrossRef]
21. Wang, Y.; Tomanek, D.; Bertsch, G.F.; Ruoff, R.S. Stability of C_{60} fullerite intercalation compounds. *Phys. Rev. B* **1993**, *47*, 6711–6720. [CrossRef]
22. Popov, A.A.; Avdoshenko, S.M.; Pendás, A.M.; Dunsch, L. Bonding between strongly repulsive metal atoms: An oxymoron made real in a confined space of endohedral metallofullerenes. *Chem. Commun.* **2012**, *48*, 8031–8050. [CrossRef]
23. Fu, W.; Zhang, J.; Fuhrer, T.; Champion, H.; Furukawa, K.; Kato, T.; Mahaney, J.E.; Burke, B.G.; Williams, K.A.; Walker, K.; et al. $Gd_2@C_{79}N$: Isolation, characterization, and monoadduct formation of a very stable heterofullerene with a magnetic spin state of S = 15/2. *J. Am. Chem. Soc.* **2011**, *133*, 9741–9750. [CrossRef] [PubMed]
24. Yan, Y.; Morales-Martinez, R.; Zhuang, J.; Yao, Y.R.; Li, X.; Poblet, J.M.; Rodriguez-Fortea, A.; Chen, N. Th@D_{5h}(6)-C_{80}: A highly symmetric fullerene cage stabilized by a single metal ion. *Chem. Commun.* **2021**, *57*, 6624–6627. [CrossRef] [PubMed]
25. Meng, Q.; Abella, L.; Yang, W.; Yao, Y.R.; Liu, X.; Zhuang, J.; Li, X.; Echegoyen, L.; Autschbach, J.; Chen, N. UCN@C_s(6)-C_{82}: An Encapsulated Triangular UCN Cluster with Ambiguous U Oxidation State [U(III) versus U(I)]. *J. Am. Chem. Soc.* **2021**, *143*, 16226–16234. [CrossRef] [PubMed]
26. Dong, B.; Yu, Y.; Slanina, Z.; Wang, F.; Lian, Y.; Uhlik, F.; Feng, L. Ho_2C_2 Cluster with Flexible Configurations inside a Large C_2(61)-C_{92} Cage. *Inorg. Chem.* **2022**, *61*, 605–612. [CrossRef] [PubMed]
27. Liu, X.; Li, L.; Liu, B.; Wang, D.; Zhao, Y.; Gao, X. Theoretical study on the ground state structure of uranofullerene U@C_{82}. *J. Phys. Chem. A* **2012**, *116*, 11651–11655. [CrossRef]
28. Mulet-Gas, M.; Abella, L.; Dunk, P.W.; Rodríguez-Fortea, A.; Kroto, H.W.; Poblet, J.M. Small endohedral metallofullerenes: Exploration of the structure and growth mechanism in the Ti@C_{2n} ($2n$ = 26–50) family. *Chem. Sci.* **2015**, *6*, 675–686. [CrossRef]
29. Li, B.; Gu, X.; Jin, P. Overlooked Effects of La-4f Orbitals in Endohedral Metallofullerenes. *Inorg. Chem.* **2022**, *61*, 5891–5902. [CrossRef]
30. Cai, W.; Alvarado, J.; Metta-Magana, A.; Chen, N.; Echegoyen, L. Interconversions between Uranium Mono-metallofullerenes: Mechanistic Implications and Role of Asymmetric Cages. *J. Am. Chem. Soc.* **2020**, *142*, 13112–13119. [CrossRef]
31. Shen, W.; Hu, Z.; Yu, P.; Wei, Z.; Jin, P.; Shi, Z.; Lu, X. An experimental and theoretical study of LuNC@$C_{76,82}$ revealing a cage-cluster selection rule. *Inorg. Chem. Front.* **2020**, *7*, 4563–4571. [CrossRef]
32. Bao, L.; Li, Y.; Yu, P.; Shen, W.; Jin, P.; Lu, X. Preferential Formation of Mono-Metallofullerenes Governed by the Encapsulation Energy of the Metal Elements: A Case Study on Eu@C_{2n} ($2n$ = 74–84) Revealing a General Rule. *Angew. Chem. Int. Ed.* **2020**, *59*, 5259–5262. [CrossRef] [PubMed]
33. Bao, L.; Peng, P.; Lu, X. Bonding inside and outside Fullerene Cages. *Acc. Chem. Res.* **2018**, *51*, 810–815. [CrossRef]
34. Xu, D.; Jiang, Y.; Wang, Y.; Zhou, T.; Shi, Z.; Omachi, H.; Shinohara, H.; Sun, B.; Wang, Z. Turning on the Near-Infrared Photoluminescence of Erbium Metallofullerenes by Covalent Modification. *Inorg. Chem.* **2019**, *58*, 14325–14330. [CrossRef]
35. Guan, R.; Chen, Z.-C.; Huang, J.; Tian, H.-R.; Xin, J.; Ying, S.-W.; Chen, M.; Zhang, Q.; Li, Q.; Xie, S.-Y. Self-driven carbon atom implantation into fullerene embedding metal–carbon cluster. *Proc. Natl. Acad. Sci. USA* **2022**, *119*, e22025631192022. [CrossRef] [PubMed]
36. Xiang, W.; Jiang, X.; Yao, Y.-R.; Xin, J.; Jin, H.; Guan, R.; Zhang, Q.; Chen, M.; Xie, S.-Y.; Popov, A.A. Monometallic Endohedral Azafullerene. *J. Am. Chem. Soc.* **2022**, *144*, 21587–21595. [CrossRef] [PubMed]
37. Li, M.; Zhao, Y.; Yuan, K.; Zhao, R.; Zhao, P.; Zhao, X. Insight into the thermodynamically preferred $V_3N@I_h$(31924)-C_{80} and acknowledged $V_xSc_{3-x}N@I_h$(31924)-C_{80} (x = 0, 1 and 2). *Carbon* **2018**, *132*, 312–322. [CrossRef]
38. Zhao, Y.-X.; Yuan, K.; Li, M.-Y.; Ehara, M.; Zhao, X. In-Depth Theoretical Probe into Novel Mixed-Metal Uranium-Based Endohedral Clusterfullerenes $Sc_2UX@I_h$(31924)-C_{80} (X = C, N). *Inorg. Chem.* **2019**, *58*, 10769–10777. [CrossRef] [PubMed]
39. Gómez-Torres, A.; Esper, R.; Dunk, P.W.; Morales-Martínez, R.; Rodríguez-Fortea, A.; Echegoyen, L.; Poblet, J.M. Small Cage Uranofullerenes: 27 Years after Their First Observation. *Helv. Chim. Acta* **2019**, *102*, e1900046. [CrossRef]

40. Raghavachari, K.; Binkley, J.S.; Seeger, R.; Pople, J.A. Self-Consistent Molecular Orbital Methods. 20. Basis set for correlated wave-functions. *J. Chem. Phys.* **1980**, *72*, 650–654.
41. Perdew, J.P.; Burke, K.; Ernzerhof, M. Generalized gradient approximation made simple. *Phys. Rev. Lett.* **1996**, *77*, 3865. [CrossRef]
42. Samoylova, N.A.; Avdoshenko, S.M.; Krylov, D.S.; Thompson, H.R.; Kirkhorn, A.C.; Rosenkranz, M.; Schiemenz, S.; Ziegs, F.; Wolter, A.U.; Yang, S. Confining the spin between two metal atoms within the carbon cage: Redox-active metal–metal bonds in dimetallofullerenes and their stable cation radicals. *Nanoscale* **2017**, *9*, 7977–7990. [CrossRef] [PubMed]
43. Popov, A.A. Redox-active metal–metal bonds between lanthanides in dimetallofullerenes. *Curr. Opin. Electrochem.* **2018**, *8*, 73–80. [CrossRef] [PubMed]
44. Glendening, E.D.; Landis, C.R.; Weinhold, F. Natural bond orbital methods. *WIREs Comput. Mol. Sci.* **2012**, *2*, 1–42. [CrossRef]
45. Frisch, M.; Trucks, G.; Schlegel, H.; Scuseria, G.; Robb, M.; Cheeseman, J.; Scalmani, G.; Barone, V.; Petersson, G.; Nakatsuji, H.; et al. *Gaussian 16, Revision A.03*; Gaussian, Inc.: Wallingford, CT, USA, 2016.
46. Bridgeman, A.J.; Cavigliasso, G.; Ireland, L.R.; Rothery, J. The Mayer bond order as a tool in inorganic chemistry. *J. Chem. Soc. Dalton Trans.* **2001**, *1*, 2095–2108. [CrossRef]
47. Popov, A.A.; Dunsch, L. Bonding in endohedral metallofullerenes as studied by quantum theory of atoms in molecules. *Chem.—Eur. J.* **2009**, *15*, 9707–9729. [CrossRef]
48. Foster, J.; Boys, S. Canonical configurational interaction procedure. *Rev. Modern Phys.* **1960**, *32*, 300. [CrossRef]
49. Lu, T.; Chen, F. Multiwfn: A multifunctional wavefunction analyzer. *J. Comput. Chem.* **2012**, *33*, 580–592. [CrossRef]